



# CHORUS

This is the accepted manuscript made available via CHORUS. The article has been published as:

## Centrifugal stretching from lifetime measurements in the $^{170}\text{Hf}$ ground state band

M. K. Smith, V. Werner, J. R. Terry, N. Pietralla, P. Petkov, Z. Berant, R. J. Casperson, A. Heinz, G. Henning, R. Lüttke, J. Qian, B. Shoraka, G. Rainovski, E. Williams, and R. Winkler

Phys. Rev. C **87**, 044317 — Published 11 April 2013

DOI: [10.1103/PhysRevC.87.044317](https://doi.org/10.1103/PhysRevC.87.044317)

# Centrifugal stretching from lifetime measurements in the $^{170}\text{Hf}$ ground state band

M. K. Smith,<sup>1,2</sup> V. Werner,<sup>1</sup> J.R. Terry,<sup>1,\*</sup> N. Pietralla,<sup>3</sup> P. Petkov,<sup>4</sup> Z. Berant,<sup>1,5</sup> R.J. Casperson,<sup>1,†</sup> A. Heinz,<sup>1,‡</sup> G. Henning,<sup>1,6,§</sup> R. Lüttke,<sup>1,3,¶</sup> J. Qian,<sup>1</sup> B. Shoraka,<sup>1,7</sup> G. Rainovski,<sup>8</sup> E. Williams,<sup>1,\*\*</sup> and R. Winkler<sup>1,\*</sup>

<sup>1</sup>Wright Nuclear Structure Laboratory, Yale University, New Haven, CT 06520-8124, USA

<sup>2</sup>Nuclear Science Laboratory, University of Notre Dame, Notre Dame, Indiana 46556, USA

<sup>3</sup>Institut für Kernphysik, Technische Universität Darmstadt, 64289 Darmstadt, Germany

<sup>4</sup>Bulgarian Academy of Sciences, Institute for Nuclear Research and Nuclear Energy, 1784 Sofia, Bulgaria

<sup>5</sup>Nuclear Research Center Negev, Beer-Sheva 84190, Israel

<sup>6</sup>ENS Cachan, 61 avenue du Président Wilson, 94235 Cachan, France

<sup>7</sup>University of Surrey, Guildford, Surrey GU2 7XH, United Kingdom

<sup>8</sup>Faculty of Physics, St. Kliment Ohridski University of Sofia, Sofia 1164, Bulgaria

Centrifugal stretching in the deformed rare-earth nucleus  $^{170}\text{Hf}$  is investigated using high-precision lifetime measurements, performed with the New Yale Plunger Device at WNSL, Yale University. Excited states were populated in the fusion-evaporation reaction  $^{124}\text{Sn}(^{50}\text{Ti},4n)^{170}\text{Hf}$  at a beam energy of 195 MeV. Recoil Distance Doppler Shift data were recorded for the ground state band through the  $J=16^+$  level. The measured  $B(E2)$  values and transition quadrupole moments improve on existing data and show increasing  $\beta$ -deformation in the ground state band of  $^{170}\text{Hf}$ . The results are compared to descriptions by a rigid rotor and by the confined  $\beta$ -soft rotor model.

PACS numbers: 21.10.Tg, 23.20.-g, 21.10.Re, 21.60.Ev

## I. INTRODUCTION

In deformed rare earth nuclei, significant deviations from rigid rotor model energy level predictions have been observed. The most obvious sign of disagreement is in the energies of rotational band members, which do not follow a simple  $J(J+1)$  rule and are a sign that the nucleus is undergoing a change in the moment of inertia with increasing angular momentum  $J$ . A change in the moment of inertia may be caused by alterations in the quadrupole ( $\beta$ ) deformation of the nucleus due to an elongation of the ellipsoid. This evolution in structure would lead to observable changes in the quadrupole moment of a given state as a function of  $J$ . Such an increase in  $\beta$ -deformation is referred to as centrifugal stretching, which has been verified in a recent study of  $^{168}\text{Hf}$  [1] through precise measurements of lifetimes of high-lying members of the ground state band (GSB). To date, centrifugal stretching has not been widely studied within the rare-earth region, especially by means of high-precision lifetime measurements, which are needed to reveal changes in transition quadrupole moments on the order of few percent. Transition quadrupole moments are an indicator for the  $\beta$ -deformation of the nucleus in its excited states. In the present work, we investigated the

even-even, more deformed neighbor isotope of  $^{168}\text{Hf}$ ,  $^{170}\text{Hf}$ .

Centrifugal stretching may only occur if the nucleus is not rigidly deformed, meaning that a certain degree of  $\beta$ -softness needs to be introduced. Many models have emerged over the past years that take this degree of freedom into account; most are based on the geometrical Bohr Hamiltonian [2],

$$H = \frac{-\hbar}{2m} \left[ \frac{1}{\beta^4} \frac{\partial}{\partial \beta} (\beta^4 \frac{\partial}{\partial \beta}) + \frac{1}{\beta^2} \frac{1}{\sin 3\gamma} \frac{\partial}{\partial \gamma} (\sin 3\gamma \frac{\partial}{\partial \gamma}) \right] - \frac{1}{4\beta^2} \sum \frac{Q_\kappa^2}{\sin^2(\gamma - \frac{2}{3}\pi\kappa)} + V(\beta, \gamma), \quad (1)$$

which is appropriate because the stretching of a nucleus refers to a geometrical phenomenon. The variables  $\beta$  and  $\gamma$  are the quadrupole shape parameters, and  $V(\beta, \gamma)$  may be approximated by an exactly separable potential such as  $V(\beta, \gamma) = \nu(\beta) + \mu(\gamma)$ . The partial derivatives in  $\beta$  and  $\gamma$  relate to the degree of softness of the potential.

Nuclear shape phase transitions have extensively been studied in recent years (see [3, 4] and Refs. therein), between spherical and deformed nuclei, as well as between prolate and oblate deformations [5]. The Bohr Hamiltonian has been used extensively to model transitional nuclei, especially on the transition paths from spherical to axially-symmetric, or to  $\gamma$ -soft nuclei. The simplest potential used was an infinite square well potential as an approximation to the potential in  $\beta$  at the critical point of the phase transition. For the spherical to axially-symmetric deformed first-order phase transition this led to the introduction of the X(5) solution [6]. Nuclei which are known to be close to this transition, i.e.  $^{150}\text{Nd}$  [7],  $^{152}\text{Sm}$  [8] and  $^{154}\text{Gd}$  [9], are known to exhibit enhanced  $\beta$ -softness, and therefore exhibit the effect of centrifugal stretching. Model calculations (e.g. in Ref. [10–12]) support the occurrence of enhanced fluctuations in  $\beta$  near the critical point also. Rare earth nuclei toward mid-shell are close to the limit of axially symmetric deformed rotors, which are algebraically

\*Present Address: Los Alamos National Laboratory, Los Alamos, New Mexico 87545, USA

†Present Address: Lawrence Livermore National Laboratory, Livermore, California 94551, USA

‡Present Address: Fundamental Physics, Chalmers University of Technology, SE-412-916 Göteborg, Sweden

§Present Address: GSI Helmholtzzentrum für Schwerionenforschung GmbH, D-64291 Darmstadt, Germany

¶Present Address: Technische Universität München, 80333 München, Germany

\*\*Present Address: Department of Nuclear Physics, Australian National University, Canberra, Australian Capital Territory 0200, Australia

classified under the SU(3) group [13]. The exact rigid rotational limit of SU(3) is never exactly realized due to a remaining width of the potential and, hence, fluctuations in  $\beta$ . Fits [14] within the interacting boson model (IBM) showed some significant deviations from the SU(3) limit - the heavier stable  $^{168-174}\text{Hf}$  isotopes were located close to the U(5)-SU(3) transition leg, near the shape-phase transitional region, involving only a small degree of  $\gamma$ -softness.

If the nuclear potential is soft in the  $\beta$  degree of freedom, level energies do not exactly follow a  $J(J+1)$  dependence as a function of angular momentum. Models like the variable moment of inertia (VMI) model [15] can account for this by varying the moment of inertia using some parametrization. In recent works within geometrical models [16–18] spin-dependent moments of inertia or mass terms were introduced in order to reproduce level schemes. The confined beta-soft (CBS) model, [19] inspired by the X(5) work of Iachello [6], varies the potential in  $\beta$  by adjusting the location of the inner wall of an infinite square well potential in  $\beta$  between the bounds of zero up to the location  $\beta_W$  of the outer wall. The effect of centrifugal stretching inherent in the CBS and other geometrical models is not due to parametrizing moments of inertia, but depends on the softness of the potential in  $\beta$ . The stretching is due to a shift in the center of mass of a state's wave function in the potential with increase of angular momentum  $J$ , not due to a variation of the potential with  $J$ . Good agreement with data was found, e.g., for  $^{168}\text{Hf}$  [1].

In the present work, we further investigated the changes of (transitional) quadrupole moments within the GSB as a function of spin through precision lifetime measurements. The new data indicate a variation in the moments of inertia due to variable quadrupole deformation, and is compared to a fit within the CBS model.

## II. EXPERIMENT AND ANALYSIS

In order to obtain information on the evolution of quadrupole deformation within the ground state rotational band, we would ideally measure the quadrupole moments of the respective excited states. Since this is a difficult task, the typical approach is to extract so-called transition quadrupole moments from reduced  $B(E2)$  transition strengths via [20]

$$Q_T(J) = \sqrt{\frac{16\pi}{5} \frac{\sqrt{B(E2; J \rightarrow J-2)}}{\langle J, 0, 2, 0 | J-2, 0 \rangle}}, \quad (2)$$

which, from comparison to geometrical models, are related to an effective  $\beta$ -deformation through

$$Q_T(J) = \frac{3}{5\pi} ZeR^2 \beta_{\text{eff}}(J), \quad (3)$$

where  $(Ze)$  is the nuclear charge and  $R$  the nuclear radius. The denominator in Eq. (2) is the Clebsch-Gordan coefficient for a given transition within the GSB. A rigid rotor has a constant transition quadrupole moment by definition. Since  $B(E2)$  values within the GSB (given that no decay-branches out of the band occur for all states of interest in this work) are

inversely proportional to lifetimes, we measured excited state lifetimes within the GSB of  $^{170}\text{Hf}$ .

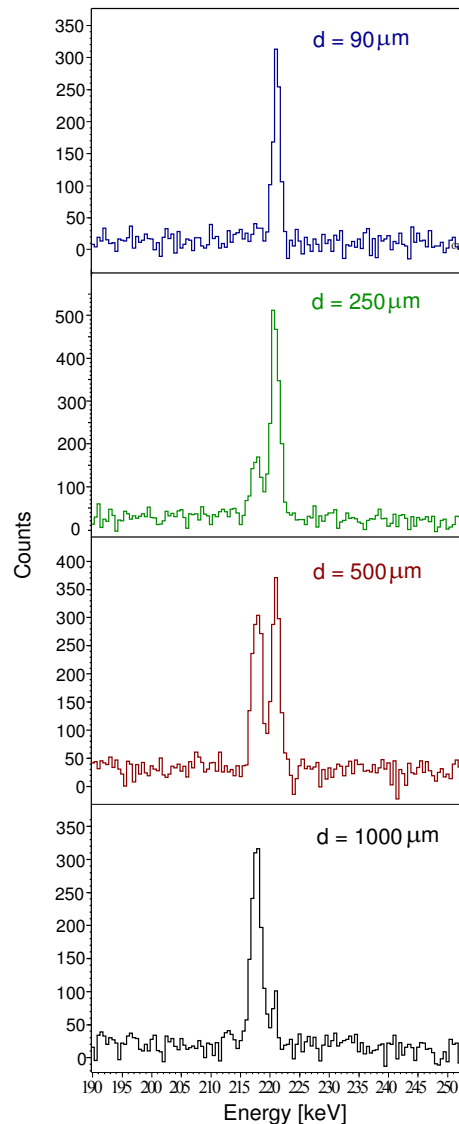


FIG. 1: (Color online) The Doppler-shifted and unshifted peaks of the 220 keV  $4_1^+ \rightarrow 2_1^+$  transition, observed in backward detectors at multiple distances after applying a gate on the shifted component of the  $6_1^+ \rightarrow 2_1^+$  transition, also in the backward detectors.

Level lifetimes and reduced transition rates for  $^{170}\text{Hf}$  were measured through a recoil distance Doppler-shift (RDDS) experiment, performed at the Wright Nuclear Structure Laboratory, Yale University. GSB excited states in  $^{170}\text{Hf}$  were populated through the  $^{124}\text{Sn}(^{50}\text{Ti}, 4n)$  fusion-evaporation reaction, with a beam delivered by the 20 MV ESTU tandem Van de Graaff accelerator at an energy of 195 MeV. The 1.0 mg/cm<sup>2</sup> thick  $^{124}\text{Sn}$  target was mounted in the Yale plunger device [21], followed by a Au stopper foil of 13mg/cm<sup>2</sup> thickness, which stopped recoiling reaction products and let the beam pass into a lead beam-dump. Coincident (minimum 2-fold)  $\gamma$ -rays were detected by clover detectors from the YRAST-Ball

array [22] at the SPEEDY setup [23], and recorded as list-mode data. Beam currents were limited to ca. 3 nA (0.72 pA) at small target-to-stopper distances, up to ca. 6 nA (0.54 pA) at larger distance settings, yielding coincidence rates of about 650–1300 Hz. Eight Compton-shielded clover detectors were mounted, four each at central polar angles  $41.5^\circ$  and  $138.5^\circ$  with respect to the beam axis. The recoil velocity of the  $^{170}\text{Hf}$  ions was approximately 1.8%  $c$ . Measurements were taken at twenty-five target-to-stopper distances;  $d(\mu\text{m}) = 2, 3, 4, 5, 7, 10, 20, 30, 40, 50, 70, 90, 110, 150, 170, 210, 250, 300, 400, 500, 600, 700, 1000, 1500$  and  $2000$ , all relative to electrical contact between the target and stopper foils. Sample spectra of the  $4_1^+ \rightarrow 2_1^+$  transition, gated on the Doppler-shifted portion of the  $6_1^+ \rightarrow 4_1^+$  transition and taken at backward angle, are shown in Fig. 1 for multiple distance settings.

Lifetimes were derived from the RDDS data using the differential decay curve method (DDCM) [24]. Since in our case we gate only on directly feeding transitions  $B$  into the states of interest, the lifetime of the state at each distance setting  $x$  is directly derived by

$$F(x) = \{B_s, A_s\}(x) \quad (4)$$

$$G(x) = \{B_s, A_u\}(x), \quad (5)$$

$$H(x) = v \frac{d}{dx} F(x), \quad (6)$$

$$\tau(x) = \frac{G(x)}{H(x)}, \quad (7)$$

where curly brackets denote a coincidence intensity,  $A$  and  $B$  denote the depopulating and feeding transitions, respectively, and  $u$  and  $s$  denote unshifted and Doppler-shifted components, respectively. Since Eq. (7) holds for each individual distance setting, an average of all values in a sensitive region is obtained, and comparison of the individual values serves as a consistency check. At each distance setting, four matrices have been constructed, corresponding to all possible combinations ( $\{138.5^\circ, 138.5^\circ\}$ ,  $\{138.5^\circ, 41.5^\circ\}$ ,  $\{41.5^\circ, 138.5^\circ\}$ ,  $\{41.5^\circ, 41.5^\circ\}$ ) of gates between forward and backward angles. The lifetimes obtained from the individual matrices serve as another consistency check to avoid systematic errors, and are subsequently averaged.

Spline curves were fitted to the data using the computer program NAPATAU [25]. The splines were fitted to the shifted intensities  $F(x)$ , and the products  $\tau \cdot H(x)$  were required to simultaneously fit the unshifted intensities  $G(x)$ . NAPATAU fits a spline of order 2 to data of shifted ( $F(x)$ ) and unshifted ( $G(x)$ ) intensities. The use of a spline is necessary, since the individual feeding paths of the state that is gated on is not known. The number of knots of the spline, which are visible as edges in the  $G(x)$  curves due to the low spline order, was kept to the necessary minimum. Examples for the fits to data from one matrix for each distance setting are given in Figs. 2 - 8. Gating in the matrices and fits to Doppler-shifted and unshifted peaks (at low energies partially overlapping) were performed using the software package TV [26].

### III. RESULTS

Lifetimes were obtained for eight states in the ground state rotational band. Gates were placed on the direct feeding transition for each of the four matrices. The first excited state at 100.8 keV,  $J^\pi = 2_1^+$ , is too long-lived for its lifetime to be derived from this experiment. The value used in this work,  $\tau(2_1^+) = 1.74(6)$  ns, was adopted from a high-precision measurement using fast timing techniques [27]. Table I gives lifetimes and  $B(E2)$  values derived in the present work. Results on the individual states are discussed in more detail below.

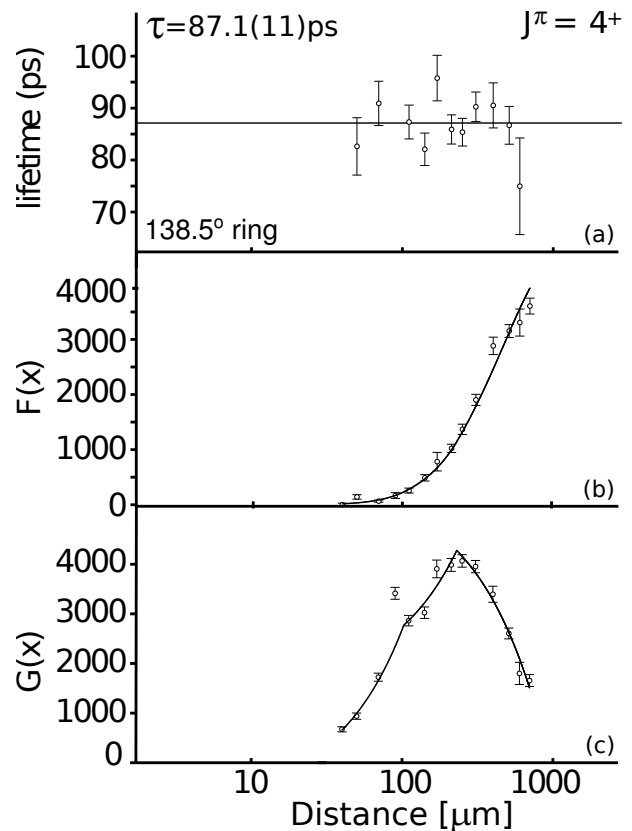


FIG. 2: DDCM analysis for the  $4_1^+$  state after gating on the backward detectors and projecting the backward spectra. (a) Lifetimes determined for each distance setting in the sensitive region, the horizontal line represents the mean value. (b) Coincidence intensities of the Doppler-shifted part of the transition from the  $4_1^+$  state and the fitted spline curve  $F(x)$  (see eq. (4)). (c) Coincidence intensities of the unshifted part of the transition and the derivative of the spline curve,  $G(x) = \tau \cdot H(x)$  [see Eqs. (5 - 7)]. The distance between the foils is given on the abscissa.

#### A. DDCM results

The  $4_1^+$  state has an energy of 322.0 keV, and decays by a 221.0 keV transition to the  $2_1^+$  state. Gating on the  $6_1^+ \rightarrow 4_1^+$  transition that directly feeds this state produces the  $\gamma - \gamma$  coincidence spectra, which are shown, for example, for back-

TABLE I: Lifetimes and  $B(E2)$  values for  $^{170}\text{Hf}$ . The conversion coefficient,  $\alpha$ , as well as the level and transition energies are taken from [28].  $B(E2)$  values are compared to those obtained in previous work.

$J^\pi$ <sup>a</sup> ( $\hbar$ )	$E_{\text{level}}(J)$ <sup>a</sup> (keV)	$E_\gamma(J \rightarrow J-2)$ <sup>a</sup> (keV)	$\tau_{\text{ThisWork}}(J)$ (ps)	$\alpha(J \rightarrow J-2)$ <sup>a</sup>	$B(E2; J \rightarrow J-2)$ (w.u.)	
					This Work	Ref. [29]
(2 <sup>+</sup> )	100.8	100.7	1740(60) <sup>b</sup>	3.47	181(6) <sup>b</sup>	178 <sup>+51</sup> <sub>-33</sub>
(4 <sup>+</sup> )	322.0	221.0	87.3(11)	0.208	263.5(33)	256 <sup>+30</sup> <sub>-25</sub>
(6 <sup>+</sup> )	642.9	320.5	13.17(42)	0.0654	309(10)	261 <sup>+24</sup> <sub>-20</sub>
(8 <sup>+</sup> )	1043.1	400.4	3.99(13)	0.0349	345(11)	301 <sup>+32</sup> <sub>-26</sub>
(10 <sup>+</sup> )	1505.2	462.2	1.81(11)	0.0238	375 <sup>+24</sup> <sub>-21</sub>	310 <sup>+44</sup> <sub>-34</sub>
(12 <sup>+</sup> )	2016.1	510.9	1.09(13)	0.0185	379 <sup>+51</sup> <sub>-40</sub>	283 <sup>+42</sup> <sub>-33</sub>
(14 <sup>+</sup> )	2567.0	550.7	0.76(11)	0.0154	375 <sup>+63</sup> <sub>-47</sub>	300 <sup>+85</sup> <sub>-54</sub>
(16 <sup>+</sup> )	3151.3	584.4	0.55(13)	0.0133	385 <sup>+119</sup> <sub>-73</sub>	~ 331

<sup>a</sup> From the NNDC database [28]

<sup>b</sup> From Ref. [27]

ward detectors in Fig. 1. A contaminant peak underneath the Doppler-shifted  $4_1^+ \rightarrow 2_1^+$  peak was found at backward angles. Thus, in this case, the lifetime of  $\tau(4_1^+) = 87.3(11)$  ps was derived from the gated forward-angle spectra via fits of both the stopped and shifted peak components over all possible distances and subsequent DDCM analysis (see Fig. 2).

The  $6_1^+ \rightarrow 4_1^+$  transition has an energy of 320.5 keV. Gates on both the forward and backward shifted components of the  $8_1^+ \rightarrow 6_1^+$  transition at 400.4 keV result in spectra with low background and good statistics similar to those for the 221.0-keV transition. An example for the DDCM analysis is shown in Fig. 3. The averaged and adopted lifetime for the  $6_1^+$  state is  $\tau(6_1^+) = 13.17(42)$  ps.

The lifetime of the  $8_1^+$  state was analyzed in the same way, by gating on the shifted components of the  $10_1^+ \rightarrow 8_1^+$  transition at 462.2 keV. An example for the DDCM analysis is shown in Fig. 4. The resulting lifetime is  $\tau(8_1^+) = 3.99(13)$  ps.

At energies above 500 keV the  $\gamma$ -ray density becomes larger, and most  $\gamma$ -rays from higher-lying states are fully Doppler-shifted and, hence, -broadened. Therefore, gates were carefully chosen in order not to include any not directly feeding transitions. The  $10_1^+ \rightarrow 8_1^+$  transition was then analyzed with the same method as the transitions below, after gating on the Doppler-shifted components of the  $12_1^+ \rightarrow 10_1^+$  transition at 510.9 keV, yielding an adopted lifetime of  $\tau(10_1^+) = 1.81(11)$  ps. An example of the DDCM fit is shown in Fig. 5.

## B. DSA corrected DDCM results

The experimental lifetimes of the high-lying ground state band levels with  $J^\pi = 12^+ - 16^+$  are  $\leq 1$  ps. The smallest plunger distances ( $d < 40 \mu\text{m}$ ) are the most sensitive, and thus DDCM-derived lifetimes are subject to an additional systematic complication due to the slow-down process in the stopper material, which is about 1.3 ps according to Monte Carlo simulations. The contribution of the line shape of unshifted peaks,

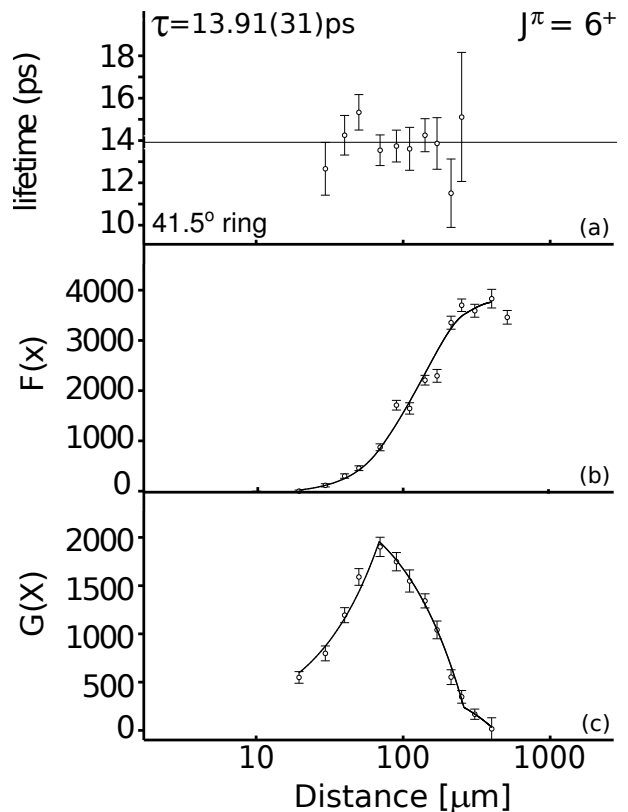


FIG. 3: Same as Fig. 2, but for the  $6_1^+$  state after gating on the backward detectors and projecting the forward spectra.

i.e. the amount of Doppler-shifted counts acquired during the stopping process, is not negligible for the range of lifetimes  $\leq 1$  ps [30]. For the states with  $J > 10$  a Doppler-shift attenuation (DSA) correction was performed via a Monte Carlo simulation of the stopping process over several thousand events. The simulation accounts for a velocity distribution after the target and the subsequent time evolution, including the stopping process in the stopper. The DDCM lifetimes were then

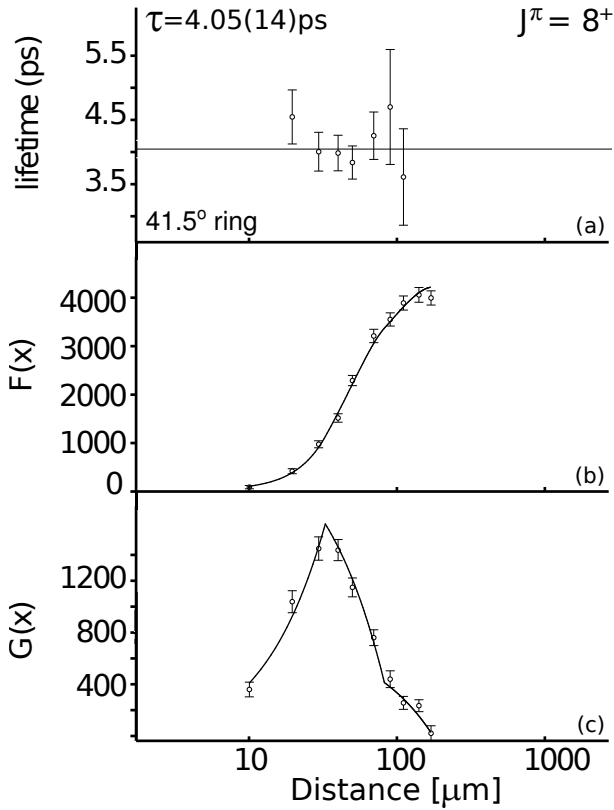


FIG. 4: Same as Fig. 2, but for the  $8_1^+$  state after gating on the backward detectors and projecting the forward spectra.

corrected by the results of this approach [30]. The first part of the analysis for these states continues as outlined above, with gated spectra produced for all four matrix combinations. DDCM lifetimes were then used as input for the DSA simulations. We add another error of 10 % in quadrature to the statistical errors to account for uncertainties in stopping powers, choice of background, etc. Table II summarizes the lifetimes obtained before and after DSA corrections.

TABLE II: Lifetimes of short lived states obtained from the straight-forward DDCM analysis, compared to DSA-corrected values. Errors of the corrected values are statistical plus a 10 % systematic error, which was added in quadrature.

$J(\hbar)$	DDCM lifetime	DSA corrected lifetime
$12^+$	0.99 (6)	1.09 (13)
$14^+$	0.59 (10)	0.76 (11)
$16^+$	0.42 (8)	0.55 (13)

The lifetime of the  $12_1^+$  state at 2016.1 keV was analyzed through gates on the Doppler-shifted components of the  $14_1^+ \rightarrow 12_1^+$  transition at 550.7 keV and analyzing Doppler-shifted and unshifted components of the  $12_1^+ \rightarrow 10_1^+$  transition. An example for the DDCM fit is shown in Fig. 6, yielding a value of 0.99(6) ps, whereas the DSA corrected value for the lifetime is  $\tau(12_1^+) = 1.09(13)$  ps.

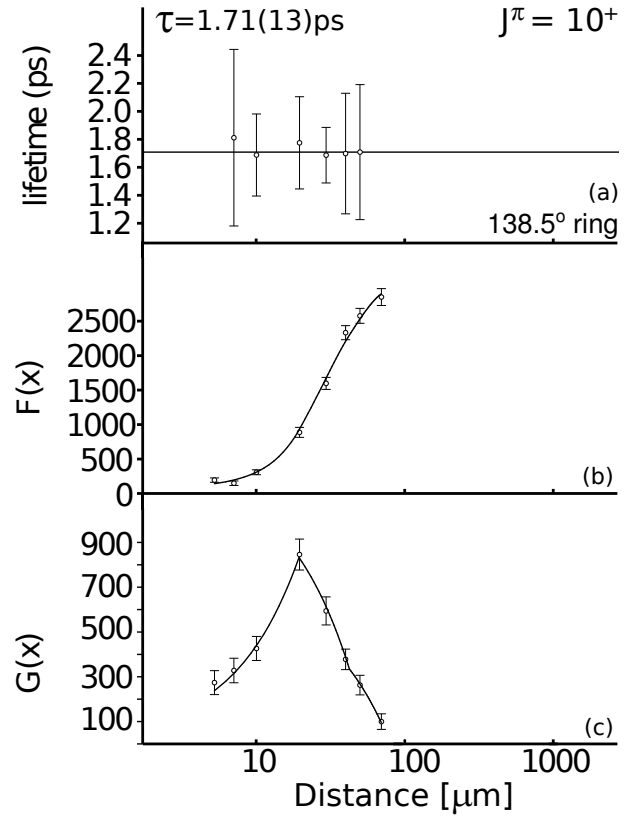


FIG. 5: Same as Fig. 2, but for the  $10_1^+$  state after gating on the forward detectors and projecting the backward spectra.

In order to obtain a fit for the  $14_1^+ \rightarrow 12_1^+$  transition, a gate was placed on the Doppler-shifted part of the  $16_1^+ \rightarrow 14_1^+$  transition at 584.4 keV. Due to the occurrence of many  $\gamma$ -ray transitions in this region, gates were very narrow. The backward shifted component of the 584.4 keV transition occurs at the same energy as a transition in  $^{197}\text{Au}$ , which is excited through Coulomb excitation on the stopper, at 576 keV. The corresponding  $J = 5/2^+$  state in Au can decay directly to the ground state with a 279.0 keV transition, or may decay to the  $J = 1/2^+$  level at 77.35 keV. Since the transition energy of interest in  $^{170}\text{Hf}$  is far from those energies, gating on these transitions in Au has no effect in the analysis. The DDCM analysis (example shown in Fig. 7) for the  $14_1^+$  state yields a lifetime of 0.59(10) ps, which is DSA corrected to  $\tau(14_1^+) = 0.76(11)$  ps.

The highest-lying state that we were able to obtain a lifetime for is the  $16_1^+$  state at 3151.3 keV. After gating on the Doppler-shifted  $18_1^+ \rightarrow 16_1^+$  transition of 615.2 keV, the DDCM analysis of the  $16_1^+ \rightarrow 14_1^+$  transition in all matrices (example shown in Fig. 8) yields a lifetime of 0.42(8) ps, which is corrected for DSA to  $\tau(16_1^+) = 0.55(13)$  ps.

In general, the average lifetime values obtained in the present work are consistently below the values from a previous RDDS experiment restricted to  $\gamma$ -ray singles measurements by Bochev *et al.* [29], although not always outside of the individual error bars. Hence,  $B(E2)$  values are higher than literature values. This effect could hint at the possibil-

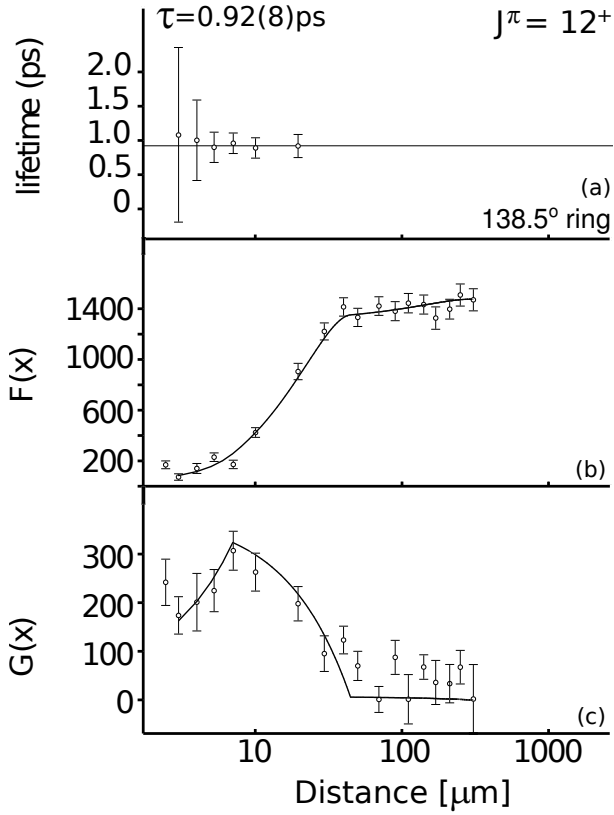


FIG. 6: Same as Fig. 2, but for the  $12_1^+$  state after gating on the forward detectors and projecting the backward spectra.

ity of incorrect incorporation of indirect (unobserved) feeding in the previous work [29], where the data could not be cleaned from background contaminants by  $\gamma\gamma$ -coincidence requirements. In the present work, side-feeding was explicitly excluded by applying coincidence gates on directly feeding transitions, therefore no assumptions of indirect feeding were necessary.

#### IV. DISCUSSION

Nuclei in this transitional region between spherical vibrators and axially symmetric rotors can be characterized by the energy ratio of the lowest excited states of the rotational ground state band,  $R_{4/2} = E(4_1^+)/E(2_1^+)$ . For spherical vibrators one expects  $R_{4/2} = 2.0$ , for an X(5)-like system  $R_{4/2} = 2.90$ . The region past the transitional point is characterized by values of  $2.90 \leq R_{4/2} \leq 3.33$ , where the latter value is the limiting case for the rigid rotor, corresponding to the expression

$$E_{RR} = \frac{\hbar^2}{2\mathcal{I}_{RR}} J(J+1), \quad (8)$$

where  $\mathcal{I}_{RR}$  is a (constant) moment of inertia. For even-even nuclei, all of the excitation energy of low-lying members of the ground state band can be attributed to rotation.

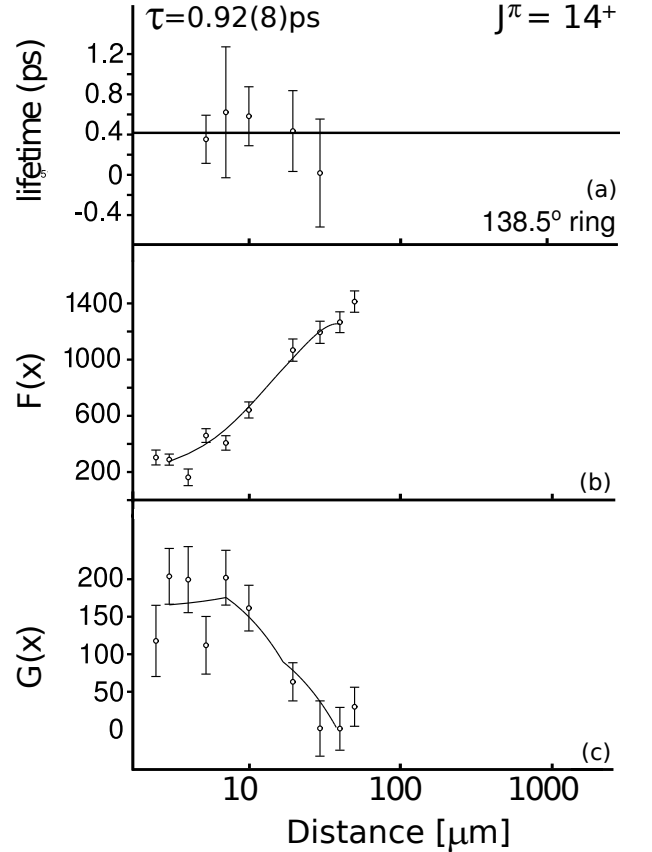


FIG. 7: Same as Fig. 2, but for the  $14_1^+$  state after gating on the forward detectors and projecting the backward spectra.

In the CBS model, the nuclear potential is approximated as an infinite square well with fixed positions of the inner wall at deformation  $\beta_<$ , and of the outer wall at deformation  $\beta_W$ . The amount of centrifugal stretching along an entire rotational band inherent to the model is dependent on one variable,  $r_\beta$ , the ratio between the position of the inner and outer walls,

$$r_\beta = \beta_</\beta_W. \quad (9)$$

Thus,  $r_\beta$  is constrained between 0 [corresponding to the X(5) solution] and 1 [rigid rotor] and, thereby, interpolates between these solutions of the Bohr Hamiltonian. The ratio was fitted to the excitation energies in the GSB of  $^{170}\text{Hf}$ , giving  $r_\beta = 0.274$ . For the GSB, the CBS model [19] gives eigenvalues of

$$E(J) = \frac{\hbar^2}{2B\beta_W^2} \left[ (z_{J,1}^{r_\beta})^2 - (z_{0,1}^{r_\beta})^2 \right], \quad (10)$$

where  $z_{J,1}^{r_\beta}$  are the first zeros of combinations of first and second order Bessel functions, as found in detail in Ref. [19]. The fit was performed to energy ratios, avoiding the absolute scale introduced by  $B$  in Eq. (10).  $B(E2)$  values in the CBS rotor model are obtained using the  $E2$  transition operator

$$\hat{T}(E2) = e_{\text{eff}} \hat{\beta}, \quad (11)$$

with an effective charge  $e_{\text{eff}}$ . Since the focus of this work is on the investigation of centrifugal stretching, we consider the

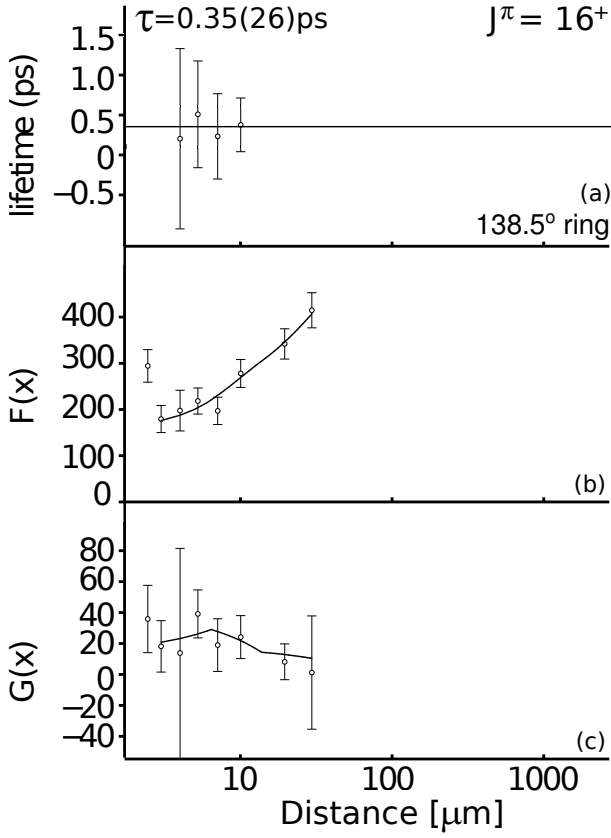


FIG. 8: Same as Fig. 2, but for the  $16_1^+$  state after gating on the forward detectors and projecting the backward spectra.

evolution of the relative moments of inertia

$$R_{\mathcal{I}(J)} = \frac{\mathcal{I}(J)}{\mathcal{I}(2_1^+)} \quad (12)$$

and of relative  $Q_T$  values

$$R_{Q_T(J)} = \frac{Q_T(J)}{Q_T(2_1^+)}. \quad (13)$$

The  $R_{\mathcal{I}(J)}$  values are related to energy ratios by

$$R_{\mathcal{I}(J)} = \frac{J(J+1)}{6} \frac{E(2_1^+)}{E(J)}. \quad (14)$$

$R_{\mathcal{I}(J)}$ -values from experiment and CBS fit are compared in Fig. 9 for the GSB members up to  $J = 16$ . The CBS values are in excellent agreement with data, clearly showing a rise of the moments of inertia toward high spins, hence, centrifugal stretching. The disagreement with data at  $J \sim 14$  is likely due to the extreme assumption of an infinite potential wall at  $\beta_W$ , whereas a realistic potential would likely have some slope and hence somewhat larger softness at high spins.

Our new lifetimes are sufficiently precise, especially for the low-spin members of the GSB, to allow for a meaningful quantitative comparison of  $B(E2)$  values within the GSB.  $R_{Q_T}$  ratios derived from experiment are shown in Fig. 10, and

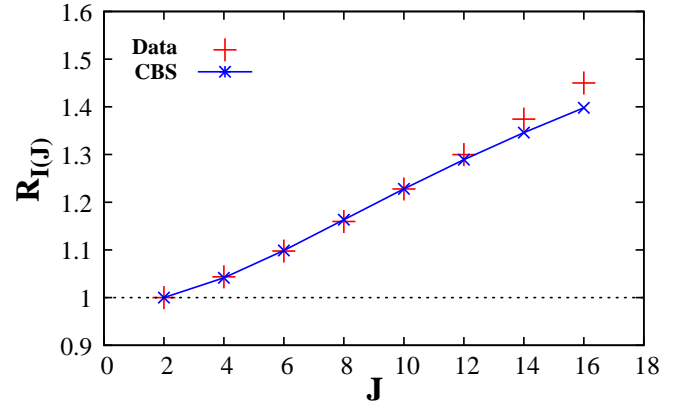


FIG. 9: (Color online) Relative moments of inertia as a function of spin. The dashed horizontal line represents the rigid rotor, the data points (red crosses) are the moments of inertia obtained from transition energies, compared to CBS values (blue stars, connected by lines for visualization).

show a significant and systematic increase from unity with increasing spin. Hence, the effect of centrifugal stretching is directly observed from transition quadrupole moments, which provide direct access to the effective  $\beta$ -deformation. Results from the CBS fit are included in Fig 10. Again, the CBS rotor model is in agreement with data. The structural parameter of  $r_\beta = 0.274$  which was fitted to excitation energies is close to the value of 0.222 which was found for the neighboring  $^{168}\text{Hf}$ . The increase of  $r_\beta$  from  $^{168}\text{Hf}$  toward  $^{170}\text{Hf}$  reflects the increase of the stiffness of the potential.

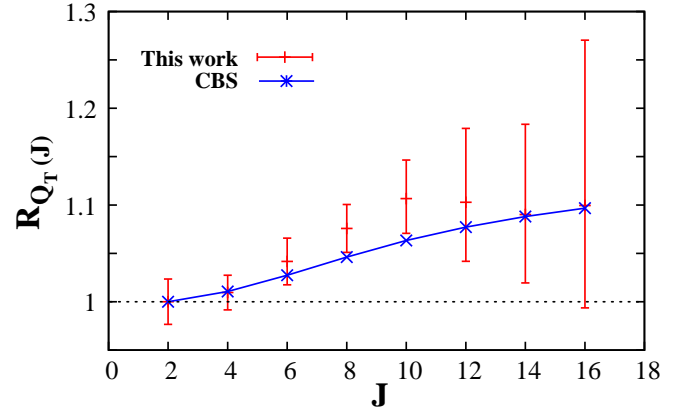


FIG. 10: (Color online) Relative transitional quadrupole moments as a function of spin. The dashed horizontal line represents the rigid rotor. The CBS description (blue stars) agrees very well with data (red crosses).

Within the GSB, the stretching is visible [12, 31] in the wavefunction densities, plotted in Fig. 11. The center of gravity of the wavefunctions is pushed to the outer wall of the potential with increasing angular momentum. Hence, centrifugal stretching is an effect of the finite width of the potential.

Data and the CBS model fit show clearly that  $^{170}\text{Hf}$  is not a

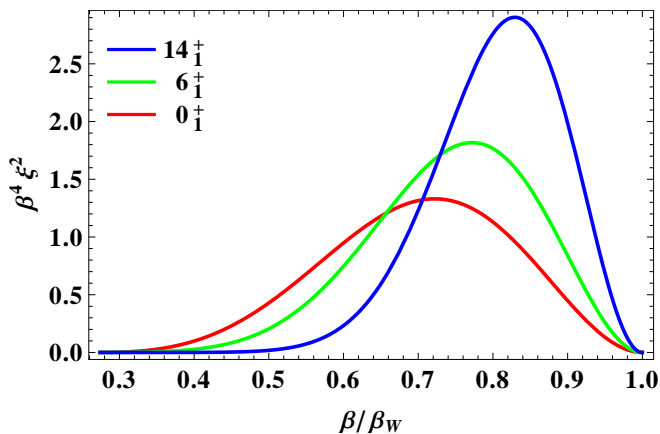


FIG. 11: (Color online) Wave function densities (see Ref. [19]) of the  $0_1^+$ ,  $6_1^+$  and  $14_1^+$  states (bottom to top curve, respectively) in  $^{170}\text{Hf}$ , calculated from the CBS model. The centers of gravity are pushed to larger deformation with increasing angular momentum.

$\beta$ -rigid rotor, but rather has a high degree of  $\beta$ -softness. This is despite the large  $R_{4/2}$  value of 3.2, very close to the rigid rotor limit of 3.33. Moments of inertia, as well as the new data for  $Q_T$  values, follow the CBS model values almost perfectly, with a relatively small choice of the softness parameter  $r_\beta$  of 0.274, fitted to reproduce the  $R_{4/2}$  ratio.

## V. CONCLUSION

We found from the measurement of transitional quadrupole moments of excited states in the GSB of  $^{170}\text{Hf}$  that  $Q_T$  val-

ues increase with spin. This directly relates to an increase of the effective  $\beta$ -deformation within the GSB. This effect, called centrifugal stretching, does not agree with the picture of a rigid rotor, but points to a certain degree of softness in the nuclear potential. The interpretation of the  $Q_T$  result agrees with increasing moments of inertia within the GSB, as inherent to the CBS rotor model. This structural characterization of Hf nuclei around  $A \approx 170$  is in good agreement with previous descriptions within the IBM [14], locating these isotopes close to the spherical-deformed phase transition where  $\beta$ -softness is enhanced.

The accuracy of the CBS rotor model is a remarkable result, with only one structural parameter controlling the width of an infinite square well potential. Our result strengthens the applicability of the CBS rotor model to nuclei which are transitional between spherical and axially-symmetric deformed nuclei, past the critical value of the phase transition on the deformed side.

## Acknowledgments

The authors thank R.F. Casten for discussions of the results, and M.K.S. thanks D. McCarthy for valuable discussions during data analysis. Help from the staff of Wright Nuclear Structure Lab is gratefully acknowledged. This work was supported in part by the U.S. DOE under Grant No. DE-FG02-91ER-40609. V.W. acknowledges support by HIC for FAIR within the LOEWE program by the state of Hesse.

- 
- [1] A. Costin, M. Reese, H. Ai, R. F. Casten, K. Dusling, C. R. Fitzpatrick, G. Gürdal, A. Heinz, E. A. McCutchan, D. A. Meyer, et al., *Phys. Rev. C* **79**, 024307 (2009).
  - [2] A. Bohr, *Kong. Dansk. Vid. Selsk.* **26** (1952).
  - [3] R. F. Casten, *Prog. Part. Nucl. Phys.* **62**, 183 (2009).
  - [4] P. Cejnar and J. Jolie, *Prog. Part. Nucl. Phys.* **62**, 210 (2009).
  - [5] J. Jolie, P. Cejnar, R. F. Casten, S. Heinze, A. Linnemann, and V. Werner, *Phys. Rev. Lett.* **89**, 182502 (2002).
  - [6] F. Iachello, *Phys. Rev. Lett.* **87**, 052502 (2001).
  - [7] R. Krücken, B. Albanna, C. Bialik, R. F. Casten, J. R. Cooper, A. Dewald, N. V. Zamfir, C. J. Barton, C. W. Beausang, M. A. Caprio, et al., *Phys. Rev. Lett.* **88**, 232501 (2002).
  - [8] R. F. Casten and N. V. Zamfir, *Phys. Rev. Lett.* **87**, 052503 (2001).
  - [9] D. Tonev, A. Dewald, T. Klug, P. Petkov, J. Jolie, A. Fitzler, O. Möller, S. Heinze, P. von Brentano, and R. F. Casten, *Phys. Rev. C* **69**, 034334 (2004).
  - [10] E. Williams, R. J. Casperson, and V. Werner, *Phys. Rev. C* **82**, 054308 (2010).
  - [11] T. Nikšić, D. Vretenar, G. A. Lalazissis, and P. Ring, *Phys. Rev. Lett.* **99**, 092502 (2007).
  - [12] A. Krugmann, Z. P. Li, J. Meng, N. Pietralla, and D. Vretenar, *J. Phys. G: Nucl. Part. Phys.* **38**, 065102 (2011).
  - [13] F. Iachello and A. Arima, *The Interacting Boson Model* (Cambridge University Press, Cambridge, 1987).
  - [14] E. A. McCutchan, N. V. Zamfir, and R. F. Casten, *Phys. Rev. C* **69**, 064306 (2004).
  - [15] M. A. J. Mariscotti, G. Scharff-Goldhaber, and B. Buck, *Phys. Rev.* **178**, 1864 (1969).
  - [16] R. V. Jolos and P. von Brentano, *Phys. Rev. C* **79**, 044310 (2009).
  - [17] D. Bonatsos, P. Georgoudis, D. Lenis, N. Minkov, and C. Quesne, *Phys. Lett. B* **683**, 264 (2010).
  - [18] D. Bonatsos, P. E. Georgoudis, D. Lenis, N. Minkov, and C. Quesne, *Phys. Rev. C* **83**, 044321 (2011).
  - [19] N. Pietralla and O. M. Gorbachenko, *Phys. Rev. C* **70**, 011304 (2004).
  - [20] J. A. Sheikh, Y. Sun, and R. Palit, *Phys. Lett. B* **507**, 115 (2001).
  - [21] R. Krücken, *J. Res. Nat. Inst. Stand. Technol.* **105**, 53 (2000).
  - [22] C. W. Beausang, C. J. Barton, M. A. Caprio, R. F. Casten, J. R. Cooper, R. Krücken, B. Liu, J. R. Novak, Z. Wang, M. Wilhelm, et al., *Nucl. Inst. Meth. Phys. Res. A* **452**, 431 (2000).
  - [23] D. Poenaru and S. Stoica, eds., *Proc. Int. Symp. Adv. Nucl. Phys.* (World Scientific, Singapore, 2000).
  - [24] A. Dewald, S. Harissopulos, and P. von Brentano, *Z. Phys. A* **334**, 163 (1989).

- [25] Program NAPATAU, University of Cologne (unpublished).
- [26] Program TV, University of Cologne (unpublished).
- [27] A. Costin, T. Ahn, B. Bochev, K. Dusling, T. C. Li, N. Pietralla, G. Rainovski, and W. Rother, *Phys. Rev. C* **74**, 067301 (2006).
- [28] C. M. Baglin, *Nucl. Data Sheets* **96**, 611 (2002).
- [29] B. Bochev, S. Iliev, R. Kalpakchieva, S. Karamian, T. Kutsarova, E. Nadjakov, and T. Venkova, *Nucl. Phys. A* **282**, 159 (1977).
- [30] P. Petkov, D. Tonev, J. Gableske, A. Dewald, T. Klemme, and P. von Brentano, *Nucl. Inst. Meth. Phys. Res. A* **431**, 208 (1999).
- [31] K. Dusling and N. Pietralla, *Phys. Rev. C* **72**, 011303(R) (2005).